Pt monolayer shell on hollow Pd core electrocatalysts: scale up synthesis, structure, and activity for the oxygen reduction reaction[•]

MIOMIR B. VUKMIROVIC[1], YU ZHANG[1], JIA X. WANG[1], DAVID BUCETA[1#], LIJUN WU[2] and RADOSLAV R. ADZIC[1*]

[1]*Chemistry Department, Brookhaven National Laboratory, Upton, NY 11973, USA and* [2]*Condensed Matter Physics & Materials Science Department, Brookhaven National Laboratory, Upton, NY 11973, USA*

Abstract: The synthesis, characterization and kinetics of the oxygen reduction reaction (ORR) of a Pt monolayer shell on Pd(hollow), or Pd–Au(hollow) core electrocatalysts are reported. Comparisons between the ORR catalytic activity of the electrocatalysts with hollow cores and those of Pt solid and Pt hollow nanoparticles were obtained using the rotating disk electrode technique. Hollow nanoparticles were made using Ni or Cu nanoparticles as sacrificial templates. The Pt ORR specific and mass activities of the electrocatalysts with hollow cores were found to be considerably higher than those of the electrocatalysts with solid cores. This enhanced Pt activity is attributed to the smooth surface morphology and hollow-induced lattice contraction. In addition, the hollow particles have a mass-saving geometry.

Keywords: platinum overlayer, electrocatalysis, fuel cells, surface strain.

INTRODUCTION

The rapidly increasing demand for fossil fuels used in transportation and power generation, and their detrimental environmental effects, have resulted in a wide-spread challenge for the development of renewable energy technologies. Fuel cells are one of the most promising clean energy technologies, particularly attractive for automobile applications, due to their high efficiency, high energy density, and low or zero emissions. The most challenging problem of their application is the slow kinetics of oxygen reduction reaction (ORR) at fuel cell

cathodes, even on Pt - the best single element electrocatalyst, which causes a large loss of the cell voltage, resulting in significant efficiency loss. In addition, Pt dissolves under certain operating condition of fuel cells. To mitigate these two drawbacks, catalysts containing large amounts of expensive Pt are required. This is one of the main reasons for the slow commercialization of fuel cells.

The ORR is a complex multi-step reaction involving the exchange of four electrons and four protons, the detailed mechanism of which still defies formulation.[1,2] Irrespective of the microscopic mechanism, a four electron process must involve the breakage of O–O bonds and the formation of O–H bonds.[1,2] According to the Sabatier principle,[3] the optimal catalyst should have moderate binding properties, such that both hydrogenation of O/OH and O–O scission are active. Density functional theory (DFT) calculations showed[4,5] that pure Pt is active for O–O scission, but hydrogenation of O/OH is slow. Therefore, weakening O and OH binding will improve ORR activity of Pt.

To address these drawbacks, the use of Pt monolayer (Pt_{ML}) electrocatalysts was proposed to reduce the cost of Pt while attempting to enhance their ORR activity and stability.[6,7] Such catalysts, consisting of a monolayer of Pt on a substrate of another material, minimize the amount of Pt while ensuring that all Pt atoms are available at the surface for catalytic activity.[6,7] Additionally, through geometric and electronic interactions with the substrate,[8,9] a Pt_{ML} can change its electronic properties and be more active and durable than pure Pt electrocatalysts.

The role of substrate (core) in determining the activity of a Pt_{ML}(shell), as a way to fine tune the balance between breaking of O–O bonds and the formation of O–H bonds, was first demonstrated in studies of the ORR, in both acid and alkaline media, on Pt_{ML} deposited on five different single-crystal surfaces (Au, Ir, Rh, Pd and Ru) and confirmed with nanoparticle supports.[7,10–12] Variations in ORR activity could be accounted for by the oxygen binding energy, which must be tuned to intermediate strength. This leads to a classic catalysis 'volcano plot' of ORR activity *vs*. oxygen binding energy, with Pt_{ML} on Pd(111) at the top of the volcano plot, having a higher ORR activity than Pt(111).[10] In addition, a fuel cell test showed that Pt_{ML} on Pd electrocatalysts was more durable than a pure Pt electrocatalyst.[13] However, further improvements in activity and durability are desirable.

Since oxygen binding energy appears to be the major descriptor of the ORR kinetics, DFT calculations suggests that further enhancement in ORR activity of Pt_{ML} on Pd could be accomplished by weakening the O and OH binding energies.[10] This could be achieved by additional contraction of the Pt_{ML} shell. A hollow core is an interesting structure to investigate geometric interaction between the Pt_{ML} shell and the core because a hollow core may induce a desirable lattice contraction of a Pt_{ML}, leading to improved ORR activity by reducing the oxygen

binding energy. In this paper, how the oxygen binding energy could be modified using a Pd hollow core is explored. The results are compared with those obtained with hollow Pt nanoparticles in order to elucidate the geometric and electronic interactions between the Pt_{ML} shell and the Pd core.

EXPERIMENTAL

Pt and Pd–Au hollow nanoparticles were obtained using Ni as a sacrificial template. First, a thin-film carbon electrode was prepared by pipetting a 15-μL aliquot of a 1 mg mL^{-1} aqueous suspension of carbon powder (Vulcan 72C) onto a polished glassy carbon surface of a rotating disk electrode (5 mm diameter, 0.196 cm^2, Pine Instrument). Then, the as-prepared thin-film electrode was immersed in a deaerated solution of 0.1 M $NiSO_4$ and 0.5 M H_3BO_3, and Ni nanoparticles were created on the carbon support by application of a double potential pulse, typically about 0.4 s at –1.4 V and 20 s at –0.8 V (*vs.* Ag/AgCl, 3 M NaCl). Once the open-circuit potential of the electrode had stabilized, it was transferred into deaerated (0.05–1 mM) K_2PtCl_4 (for Pt hollow) or 0.5 mM $Pd(NH_3)_4Cl_2 + xHAuCl_4$ (for Pd–Au hollow) solutions without exposure to air, whereby the galvanic replacement of Ni by Pt or Pd and Au occurred. After 3–30 min, electrode was rinsed with water, to eliminate residual metal ions, and cycled (for about 20 cycles) from 0.05 to 1.2 V *vs.* the reversible hydrogen electrode (RHE) in a deaerated 0.1 M $HClO_4$ solution to facilitate the complete removal of the Ni atoms. The hollow Pd–Au nanoparticles were prepared with Pd-to-Au concentration ratios of 20:1 and 10:1 in the precursor solutions. They are denoted as $Pd_{20}Au(h)/C$ and $Pd_{10}Au(h)/C$, respectively. The hollow Pt nanoparticles are denoted as Pt(h)/C. The Pt_{ML} was placed on the hollow Pd–Au nanoparticles using galvanic replacement of an underpotentially deposited Cu monolayer, as previously reported.[7,14] The experimental set-up was described elsewhere.[15] These samples are designated as $Pt_{ML}/Pd_{20}Au(h)/C$ and $Pt_{ML}/Pd_{10}Au(h)/C$ respectively. The solid Pt (Pt(s)/C) and Pd (Pd(s)/C) nanoparticle samples were carbon-supported Pt (45 wt. %) and Pd (10 wt. %), respectively.

For large-scale synthesis, the carbon-supported hollow Pd nanoparticles (Pd(h)/C) were prepared by a two-step synthesis method. In the first step, Cu nanoparticles were prepared by slowly adding $NaBH_4$ into the mixture of carbon (Vulcan X72), $CuCl_2$, and Na-citrate. In the second step, $Pd(NH_3)_4Cl_2$ was added, thus forming Pd hollow nanoparticles by galvanic displacement of Cu with Pd. The procedure for one batch-synthesis of 650 mg of the $Pt_{ML}/$ /Pd(h)/C catalyst was described elsewhere.[16]

All the electrochemical treatments and measurements were performed with a Voltalab PGZ402 potentiostat (Radiometer Analytical) at room temperature. The electrolyte was 0.1 M $HClO_4$ solution. An Ag/AgCl (3 M NaCl) electrode was used as the reference electrode and a Pt flag was used as the counter electrode. All the potentials are given with respect to a RHE. The electrochemical surface area (*ESA*) was calculated using the integrated hydrogen desorption charges from cyclic voltammetry (CV) curves assuming 0.21 mC cm^{-2}.[17] Kinetic currents at 0.9 V were calculated from the ORR polarization curves using $j_k = j/(1–j/j_L)$, where j is the measured current at 0.9 V and j_L is the diffusion-limited current below 0.5 V. The obtained kinetic current was further normalized to *ESA* and Pt mass to calculate Pt specific (*SA*) and mass activities (*MA*), respectively. The currents in the voltamograms were normalized to the geometric electrode surface area.

Transmission electron microscope (TEM) imaging was realized using a JEOL 3000F TEM operating at 300 kV equipped with Gatan image filter system. The mass contents of Pd and Pt were determined using inductively coupled plasma mass spectrometry (ICP–MS)

measurements. The very small amount of Au could not be reliably determined by ICP–MS and was estimated using the measured Pd mass and the atomic ratio in the mixed Pd–Au solutions. Scanning TEM (STEM) measurements were performed using a Hitachi HD2700C microscope equipped with a cold field emission electron source and a probe aberration corrector. X-Ray diffraction (XRD) experiments were performed on a Beamline X7B (λ = = 0.3196 Å) of the National Synchrotron Light Source at Brookhaven National Laboratory. Two dimensional powder patterns were collected with a Perkin Elmer image plate detector, and the diffraction rings were integrated using the FIT2D code. The fitted parameters (lattice constant and particle size) were obtained through a Rietveld refinement. Lanthanum hexaboride (LaB_6) was used as the instrumental reference.

RESULTS AND DISCUSSION

As discussed above, hollow Pt, Pd, and Pd–Au nanoparticles were prepared by exposing Ni or Cu nanoparticles to Pt, Pd, or Pd–Au containing solutions. The formation of voids in these nanoparticles was governed by both galvanic replacement and the Kirkendall Effect (vacancy-mediated diffusion mechanism). While galvanic replacement is responsible for displacing Ni (or Cu) with Pt, Pd or Pd–Au and thus creating core–shell structure, due to Kirkendall effect, Ni (Cu) from the core can diffuse through the shell to its surface where it will be replaced with Pt, Pd, or Pd–Au. Due to the different diffusion rates of Ni (Cu) and Pt, Pd, or Pd–Au, vacancies will be generated inside the core–shell nanostructures, and they may coalesce into a single void (hollow) or multiple voids (porous).

Ni nanoparticles were found suitable as templates to facilitate the formation of single-void particles with complete Pt shells.[18] Pt hollow nanoparticle in high-resolution STEM images for the samples after electrochemical measurements are displayed in Fig. 1a. The synthetic parameters were varied in order to optimize the ORR activity and durability. The best catalytic activity was found with 3–9 nm hollow spheres with a 1–2 nm thick shell.
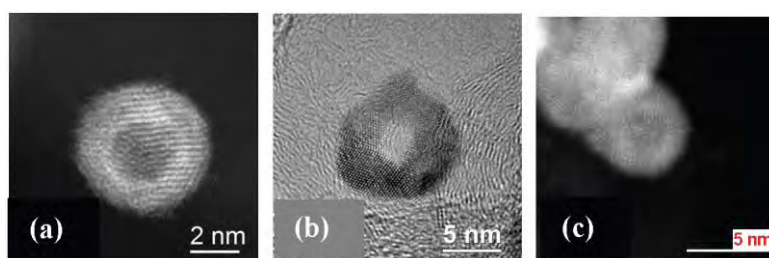
Fig. 1. a) High-resolution STEM image of a Pt(h)/C nanoparticle, b) TEM image of $Pt_{ML}/Pd_{20}Au(h)/C$ nanoparticle and c) TEM image of $Pt_{ML}/Pd(h)/C$ nanoparticle.

However, hollow structures were more difficult to form with Pd or Au ions alone when using Ni nanoparticles as sacrificial templates. Lower melting temperature of Au compared to Ni suggests that Ni diffuses slower than Au. Consequently, the voids generated by Ni atoms slowly diffusing out through the Au

shell will be filled by inward faster-diffusing Au atoms before they coalesce into a single void, thus resulting in solid Au particles. In Ni–Pd case, the difference in diffusivity between Ni and Pd is not large enough (the small difference in melting temperatures) to create sufficient vacancies to form Pd hollow nanoparticles.

The addition of Au ions in Pd solutions may mediate the diffusion process and promote the formation of hollow particles.[19] In the Pd–Au mixed solution, since the standard reduction potential of the $AuCl_4^-$/Au redox couple (1.002 V vs. SHE) is higher than that of the $Pd(NH_3)_4^{2+}$/Pd couple (0.902 V vs. SHE),[20] Au ions will be preferentially reduced instead of Pd ions and deposited on the surface of the Ni templates as a thin shell. The imbalance between the outward flux of faster-diffusing Ni–Au atoms and the inward flux of the slower-diffusing Pd atoms will be compensated for by an inward flux of vacancies. The vacancies will then supersaturate and coalesce into a single void. On the shell surface, the Ni atoms that flowed out will spontaneously dissolve because of their lower reduction potential, while the Au atoms will remain intact because of their higher reduction potential. Typical TEM images of a Pt_{ML}/$Pd_{20}Au(h)$/C sample with hollow cores are shown in Fig. 1b. The adding of a small amount of Au to the Pd core only improved the stability of Pd while its interaction with Pt_{ML} was not influenced.[13] Therefore, as long as only the core–Pt_{ML} interaction is considered, Pd–Au can be treated as Pd.

The TEM images confirmed the hollow structure of the Pd nanoparticles prepared by the large-scale synthesis method. They had a narrow size distribution with an average diameter of 5 nm and shell thickness of 1.5 nm (Fig. 1c).

The effect of the voids in nanoparticles on the ORR activity of the top Pt layer was investigated by recording the ORR polarization curves in oxygenated 0.1 M $HClO_4$ using the rotating disk electrode technique. The ORR polarization curves for Pt(h) and Pt(s) nanoparticles are shown in Fig. 2a, while the ORR polarization curves for Pt_{ML}/$Pd_{20}Au(h)$/C and Pt_{ML}/Pd(s)/C nanoparticles are presented in Fig. 2b. In both cases, solid and hollow nanoparticles show similar onset and kinetic part of the ORR polarization curve. However, the onset and half-wave potentials are not true measures of ORR activity but only qualitative indicators since they are sensitive to catalyst loading. This could be clearly seen if the respective voltammetry curves of the samples in deaerated 0.1 M $HClO_4$ are examined, Fig. 3a and b. The H adsorption–desorption charge at low potentials and the OH adsorption–desorption charge at high potentials are both smaller on the hollow than on the solid samples because the catalyst loading of the hollow samples is lower than that of the solid ones. Additionally, the hollow samples have smaller *ESA* values compared to those of the solid samples, due to their larger average particle size (Table I).

The correct way to compare the ORR activity of these catalysts is to use the Pt mass and specific activities, which compare the ORR activity of the catalysts

to the same reference point, as shown in Table I. The *SA* and *MA* values of the hollow samples were higher than those for the solid ones. The *ESA* per Pt mass (ESA_{Pt}) is similar for the solid and hollow samples. This means that the enhancement in *MA* (where $MA = SA \times ESA_{Pt}$) for hollow samples mainly results from increased *SA* values.
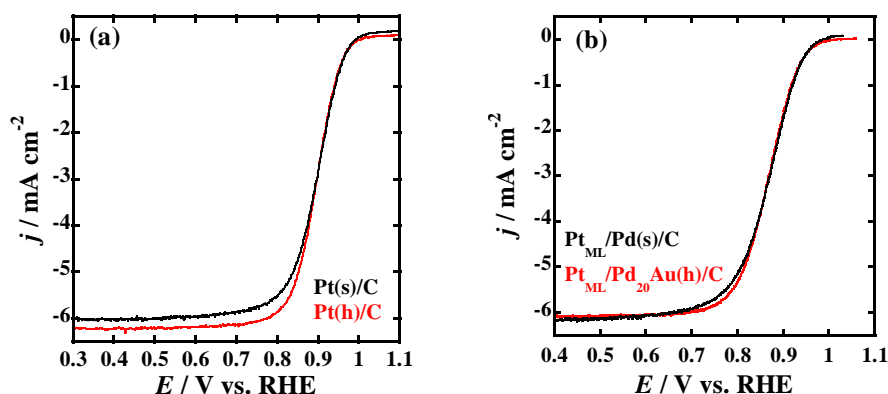
Fig. 2. ORR polarization curves in oxygen-saturated 0.1 M $HClO_4$ solutions, in the forward potential sweep at 10 mV s^{-1} with a 1600 rpm rotation rate for a) Pt(s)/C and Pt(h)/C and b) $Pt_{ML}/Pd_{20}Au(h)/C$ and $Pt_{ML}/Pd(s)/C$ nanoparticles.
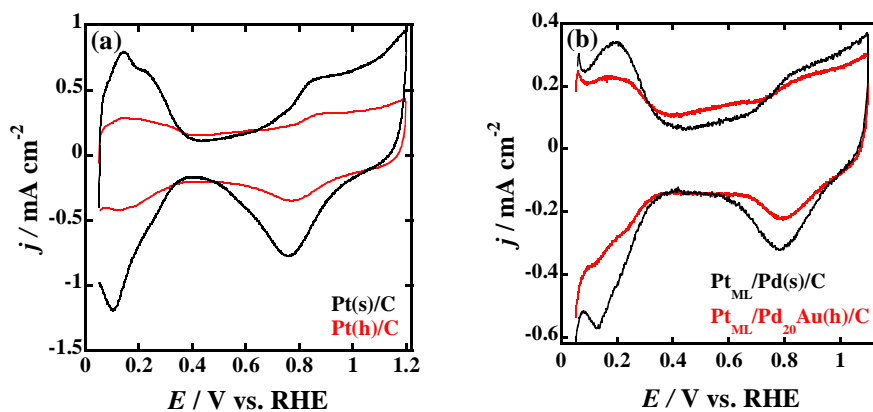
Fig. 3. Voltammetry curves in deareated 0.1 M $HClO_4$ solutions for a) Pt(s)/C and Pt(h)/C and b) $Pt_{ML}/Pd_{20}Au(h)/C$ and $Pt_{ML}/Pd(s)/C$ nanoparticles.

The oxidation of hollow samples was shifted to more positive potentials compared to those of the solid samples (Fig. 3). This indicates that the Pt–OH interaction became weaker for the hollow particles, causing an increase in their *SA*. The reduction in the coverage of the oxygen-containing species could be attributed to the smooth (Fig. 1) and void-induced contracted surface of the hollow samples. The binding energy of oxygen was decreased for the hollow samples

because the smooth surface possessed high-coordination sites that are less reactive than the low-coordination sites at the edges and defects while the hollow-induced surface contraction down-shifted the d-band center of the Pt top layer, thus making it less reactive.[8,9]

TABLE I. Particle diameter, loading, and Pt specific and mass activities for the ORR at 0.9 V in oxygen-saturated 0.1 M $HClO_4$ solutions for Pt(h)/C, Pt(s)/C, $Pt_{ML}/Pd_{20}Au(h)/C$ and $Pt_{ML}/Pd(s)/C$ nanoparticles; h = hollow, s = solid, d = particle diameter, L = loading, R_{SA} = enhancement in SA between hollow and solid nanoparticles, $cm^2_{geo.}$ = geometric area, cm^2_r = real area

Nanoparticle	D nm	L $\mu g\ cm^{-2}_{geo.}$	ESA_{Pt} $cm^2_r\ \mu g^{-1}$	SA $mA\ cm^{-2}_r$	R_{SA}	MA $mA\ \mu g^{-1}$
Pt(h)/C	6.5	5	0.64	1.71	4.275	1.1
Pt(s)/C	3.2	22	0.62	0.4		0.25
$Pt_{ML}/Pd_{20}Au(h)/C$	9	1.4 Pt 3.9 total metal	1.9	0.85	1.71	1.62
$Pt_{ML}/Pd(s)/C$	4	7 Pd	1.92	0.5		0.96

To examine the hollow-induced lattice contraction, X-ray diffraction measurements on hollow and solid nanoparticles were performed. As shown in Fig. 4, the diffraction peaks shifted to higher angles for the hollow samples compared to those of the solid ones, indicating that a smaller lattice spacing was induced by the hollow cores.
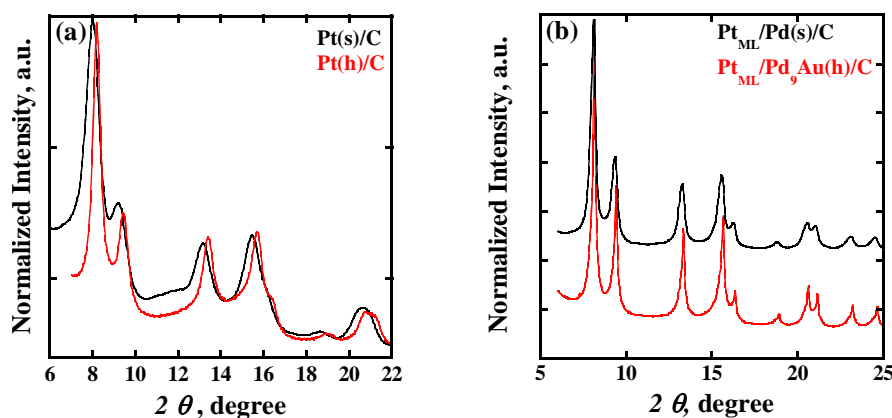
Fig. 4. X-Ray powder diffraction intensity for a) Pt(s)/C and Pt(h)/C and b) $Pt_{ML}/Pd_9Au(h)/C$ and $Pt_{ML}/Pd(s)/C$ nanoparticles.

As discussed above, in both systems, the enhancement in MA for hollow samples mainly stems from their increased SA. However, the improvement of SA for pure Pt samples is 2.5 times larger than for Pt–Pd samples (Table I). This could be explained taking into account the mechanical stress state of the top Pt

layer on Pt(s)/C and the Pt$_{ML}$ on Pd(s)/C, and that *SA* enhancement, in these cases, is only due to geometric effects. While top Pt layer on Pt(s) is neither compressed nor expanded (neglecting the effect of the small particles), the Pt$_{ML}$ on Pd(s) is compressed due to the difference in lattice constants between Pt and Pd. Therefore, the top Pt layer on Pt(h) could be compressed more than Pt$_{ML}$ on Pd$_{20}$Au(h)/C. As a result, a larger enhancement in *SA* for the pure Pt than for the Pt–Pd samples was achieved.

The durability of the Pt$_{ML}$/Pd(h)/C catalyst was tested under half-cell conditions. The potential was cycled from 0.6 to 1.0 V in naturally aerated 0.1 M HClO$_4$. A comparison of the ORR polarization curves before and after 5,000 cycles is shown in Fig. 5. The small negative shift of ORR polarization curve after 5,000 cycles indicates good stability.
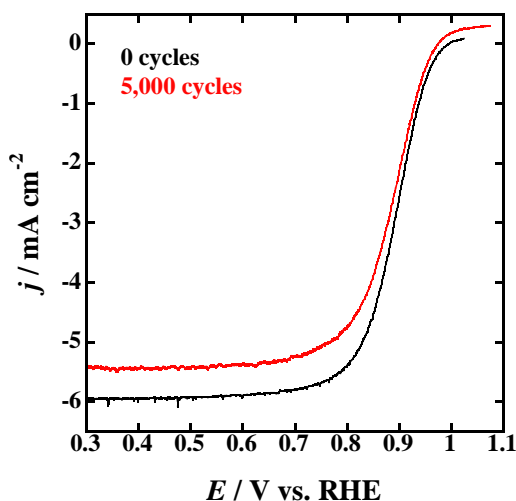
Fig. 5. ORR polarization curves in oxygen-saturated 0.1 M HClO$_4$ solutions for Pt$_{ML}$/Pd(h)/C before and after 5,000 cycles.

CONCLUSIONS

Pt$_{ML}$ on Pd(s) and Pd–Au(h) cores electrocatalysts were synthesized and characterized. Their ORR activities were examined and compared with the ORR activity of Pt(s) and Pt(h) nanoparticles. Hollow nanoparticles were made using Ni or Cu as sacrificial templates. The hollow architecture of Pt and Pd–Au nanoparticles was achieved by the delicate balance between galvanic displacement and the Kirkendall Effect in controlling the reaction kinetics. Since the *ESA* per Pt mass was similar for the solid and hollow samples, the enhancement in *MA* for the hollow samples mainly resulted from increased *SA* values. The increase in *SA* could be mainly attributed to the void-induced contracted surface of the hollow samples and partially due to the smooth surface morphology of the hollow nanoparticles. The binding energy of oxygen was decreased for the hollow samples because their smooth surface posses high-coordination sites, which are less reac-

tive than the low-coordination sites at edges and defects. Additionally, the hollow-induced surface contraction downshifted the d-band center of the Pt top layer, thus making it less reactive. The $Pt_{ML}/Pd(h)/C$ catalyst showed good durability after 5,000 potential cycles from 0.6 to 1.0 V. The hollow-induced lattice contraction provides an alternative route to fine tune the oxygen binding characteristics of surface of the catalysts toward better ORR activities.

ИЗВОД

ЕЛЕКТРОКАТАЛИЗАТОРИ СА МОНОСЛОЈНОМ Pt ЉУСКОМ НА ШУПЉЕМ ЈЕЗГРУ Pd: СИНТЕЗА, СТРУКТУРА И АКТИВНОСТ ЗА РЕАКЦИЈУ РЕДУКЦИЈЕ КИСЕОНИКА

MIOMIR B. VUKMIROVIC[1], YU ZHANG[1], JIA X. WANG[1], DAVID BUCETA[1], LIJUN WU[2] и RADOSLAV R. ADZIC[1]

[1]*Chemistry Department, Brookhaven National Laboratory, Upton, NY 11973, USA и* [2]*Condensed Matter Physics & Materials Science Department, Brookhaven National Laboratory, Upton, NY 11973, USA*

Приказана је синтеза, карактеризација и електрокаталитичка активност за реакцију редукције кисеоника (РРК) катализатора који се састоји од монослојне Pt љуске на шупљем језгру Pd или Pd–Au. За упоређење каталитичке активности катализатора са шупљим језгром и Pt катализатора (пуна Pt и шупље Pt наночестице) за РРК, коришћена је техника ротирајућег диска. Шупље наночестице добијене су коришћењем Ni или Cu наночестица као „жртвујућих" матрица. Нађено је да је специфична и масена активност Pt катализатора са шупљим језгром за РРК знатно већа него за пуно језгро. Увећана активност Pt приписана је глаткој површинској морфологији и контракцији решетке која је изазвана шупљом структуром језгра, што је додатни ефекат уз уштеду масе метала код честица са шупљином.

(Примљено 24. октобра 2013)

REFERENCES

1. R. R. Adzic, *Recent Advances in the Kinetics of Oxygen Reduction* in *Electrocatalysis*, J. Lipkowski, P. N. Ross, Eds., Wiley–VCH, New York, 1998, p. 197
2. M. R. Tarasevich, A. Sadkowsky, E. Yeager, *Oxygen Electrochemistry*, in *Comprehensive Treatise of Electrochemistry*, Vol. 7, B. E. Conway, J. O'M. Bockris, E. Yeager, S. U. M. Khan, R. E. White, Eds., Plenum Press, New York, 1983, p. 301
3. R. I. Masel, *Principles of Adsorption and Reaction on Solid Surfaces*, Wiley, New York, 1996, p. 702
4. J. K. Nørskov, J. Rossmeisl, A. Logadottir, L. Lindqvist, J. R. Kitchin, T. Bligaard, H. Jonsson, *J. Phys. Chem., B* **108** (2004) 17886
5. J. A. Herron, J. Jiao, K. Hahn, G. Peng, R. R. Adzic, M. Mavrikakis, *Electrocatalysis* **3** (2012) 192

6. R. R. Adzic, J. Zhang, K. Sasaki, M. B. Vukmirovic, M. Shao, J. X. Wang, A. U. Nilekar, M. Mavrikakis, J. A. Valerio, F. Uribe, *Top. Catal.* **46** (2007) 249
7. J. Zhang, Y. Mo, M. B. Vukmirovic, R. Klie, K. Sasaki, R. R. Adzic, *J. Phys. Chem., B* **108** (2004) 10955
8. B. Hammer, J. K. Nørskov, *Adv. Catal.* **45** (2000) 71
9. J. Greeley, J. K. Nørskov, M. Mavrikakis, *Annu. Rev. Phys. Chem.* **53** (2002) 319
10. J. Zhang, M. B. Vukmirovic, Y. Xu, M. Mavrikakis, R. R. Adzic, *Angew. Chem. Int. Ed.* **44** (2005) 2132
11. F. H. B. Lima, J. Zhang, M. H. Shao, K. Sasaki, M. B. Vukmirovic, E. A. Ticianelli, R. R. Adzic, *J. Phys. Chem., C* **111** (2007) 404
12. F. H. B. Lima, J. Zhang, M. H. Shao, K. Sasaki, M. B. Vukmirovic, E. A. Ticianelli, R. R. Adzic, *J. Solid State Electrochem.* **12** (2008) 399
13. K. Sasaki, H. Naohara, Y. Cai, Y. M. Choi, P. Liu, M. B. Vukmirovic, J. X. Wang, R. R. Adzic, *Angew. Chem. Int. Ed.* **49** (2010) 8602
14. S. R. Brankovic, J. X. Wang, R. R. Adzic, *Surf. Sci.* **474** (2001) L173
15. M. B. Vukmirovic, S. T. Bliznakov, K. Sasaki, J. X. Wang, R. R. Adzic, *Electrochem. Soc. Interface* **Summer** (2011) 33
16. K. Sasaki, J. X. Wang, H. Naohara, N. Marinkovic, K. More, H. Inada, R. R. Adzic, *Electrochim. Acta* **55** (2010) 2645
17. T. J. Schmidt, H. A. Gasteiger, G. D. Stab, P. M. Urban, D. M. Kolb, R. J. Behm, *J. Electrochem. Soc.* **145** (1998) 2354
18. J. X. Wang, C. Ma, Y. M. Choi, D. Su, Y. Zhu, P. Liu, R. Si, M. B. Vukmirovic, Y. Zhang, R. R. Adzic, *J. Am. Chem. Soc.* **133** (2011) 13551
19. Y. Zhang, C. Ma, Y. Zhu, R. Si, Y. Cai, J. X. Wang, R. R. Adzic, *Catal. Today* **202** (2013) 50
20. A. J. Bard, R. Parsons, J. Jordan, *Standard Potentials in Aqueous Solution*, M. Dekker, New York, 1985.